Warm stellar matter within the quark-meson-coupling model

P. K. Panda,[1] C. Providência,[1] and D. P. Menezes[2]

[1]*Centro de Física Computacional, Department of Physics, University of Coimbra, P-3004-516 Coimbra, Portugal*

[2]*Departamento de Física, CFM, Universidade Federal de Santa Catarina, Florianópolis - SC, CP. 476, CEP 88.040 - 900, Brazil*

(Received 26 June 2010; revised manuscript received 14 September 2010; published 18 October 2010)

In the present article, we investigate stellar matter obtained within the quark-meson-coupling (QMC) model for fixed temperature and with the entropy of the order of 1 or 2 Boltzmann units per baryon for neutrino-free matter and matter with trapped neutrinos. A new prescription for the calculation of the baryon effective masses in terms of the free energy is used. Comparing the results of the present work with those obtained from the nonlinear Walecka model, smaller strangeness and neutrino fractions are predicted within QMC. As a consequence, QMC has a smaller window of metastability for conversion into a low-mass blackhole during cooling.

DOI: 10.1103/PhysRevC.82.045801 PACS number(s): 21.65.−f, 24.10.Jv, 24.85.+p, 95.30.Tg

I. INTRODUCTION

Understanding the complete quantum chromodynamics (QCD) phase diagram and being able to reproduce all states of matter that it describes is the final goal toward the explanation of the evolution of the universe from its primordial times. Unfortunately, solving the QCD is still far from possible and physicists are left with effective theories and lattice QCD.

Effective models can be successfully applied to the description of compact-star properties in nuclear astrophysics as well as to nuclear matter and finite nuclei properties, these studies taking place at low and moderate temperatures. The knowledge of the equation of state (EOS) of nuclear matter under exotic conditions, including high-isospin asymmetries, finite temperatures, and a wide density range, is essential for our understanding of the evolution of the stars and of the nuclear force underlying the calculations. One of the most common effective models is the nonlinear Walecka model (NLWM) [1] that reproduces the nuclear binding energy at the correct saturation density by imposing that nucleons exchange scalar and vector mesons. In this model, the nucleons have no internal structure. The quark-meson-coupling (QMC) model [2] is another effective model that bears a philosophy similar to the NLWM, with the advantage that the internal structure of the nucleon is introduced explicitly. Within the QMC model, matter at low densities and temperatures is a system of nucleons interacting through meson fields, with quarks and gluons confined within MIT [3] bags. For matter at very high density or temperature, one expects that baryons and mesons dissolve and that the entire system of quarks and gluons becomes confined within a single, big, MIT bag.

The energy of the nucleonic MIT bag is identified with the effective mass of the nucleon. This identification is natural at zero temperature, but if one wants to describe a system at finite temperature, it has important implications: while in the NLWM model the nucleon mass always decreases with temperature, in the QMC it increases and may become higher than the free mass [4]. This difference arises due to the explicit treatment of the internal structure of the nucleon in the QMC. When the bag is heated up, quark-antiquark pairs are excited in the interior of the bag, increasing the internal energy of the bag.

In the present article, instead of identifying the effective mass of the nucleon with the bag energy, it is identified with the free energy of the bag, and a direct consequence is the recovery of the behavior of the NLWM for the effective mass; that is, it decreases with increasing temperature and never becomes higher than the corresponding free mass. This prescription was already employed successfully in the calculation of particle production yields on a Au + Au collision at the BNL Relativistic Heavy Ion Collider (RHIC) [5].

QMC has been used to describe cold stellar matter. In particular, it was used to investigate the properties of neutron stars with the inclusion of hyperons, quarks, and kaon condensation [6–9] as well as stellar matter subject to very strong magnetic fields [10,11]. Pure hadronic compact stars, above a threshold value of their gravitational mass, are metastable to the conversion to quark stars (hybrid or strange stars). In Ref. [12], a systematic study of the metastability of pure hadronic compact stars using different relativistic models for the equation of state, including QMC, was performed. It was shown that the QMC model has a very narrow region of metastability for pure hadronic stars. This was due to the fact that the nucleonic EOS for QMC is very soft and, therefore, the onset of hyperons occurs at quite high densities, which gives rise to large critical masses. The conversion to a quark star will occur only for a small value of the bag constant. It was also pointed out that QMC limiting masses may be as high as 1.9 $M_{\odot}$.

In Refs. [13,14] it was shown that the density dependence of the symmetry energy at saturation; namely, the symmetry energy slope and the symmetry term of the incompressibility of the nuclear EOSs at saturation, are within the constraints imposed by isospin diffusion in heavy-ion collisions [15]. Moreover, in Ref. [14], results obtained with QMC were compared thoroughly with those arising from several Skyrme, relativistic effective models, and a microscopic Brueckner Hartree-Fock calculation and the values of the parameters characterizing the QMC equation of state of isospin asymmetric nuclear matter were shown to fall within the trends predicted by those other models.

Other constraints coming from both heavy-ion collisions and the phenomenology of compact stars have been proposed

[16–18]. QMC satisfies some of these constraints. The EOS at intermediate or high densities falls within the limits imposed by heavy-ion collisions [19]. Another constraint is the one imposed by the pulsar B in the double-pulsar system J0737-3039 with a mass equal to $1.249 \pm 0.001\ M_\odot$ [16]. The low mass of this pulsar seems to indicate that it was formed in a type-I supernova of an ONeMg white dwarf, in which case we predict a baryon mass of $M_B = 1.366 - 1.375\ M_\odot$, assuming no loss of matter, or $M_B = 1.353 - 1.362\ M_\odot$ for 1% mass loss. QMC predicts $1.356\ M_\odot$ within this last mass interval. QMC fails to obey the constraint imposed by compact-star cooling observations. Within QMC, the direct Urca process occurs for densities larger than $1.04\rho_0$, which are smaller than the value $1.35\rho_0$ obtained from observation of compact-star cooling. This result is expected because the isovector channel within QMC is described too simply, giving rise to a hard symmetry energy. The QMC symmetry energy could be easily corrected by including a nonlinear $\omega\rho$ term as in Ref. [20], which would soften the symmetry energy and shift the direct Urca onset to larger densities. In Ref. [17], a constraint on the radius of neutron stars ($T = 0$) is imposed by microscopic calculations based on chiral effective-field theory. The authors show that, for a star with $M = 1.4\ M_\odot$, the radius should be $R = 11.8 \pm 2.1$ km. QMC predicts 13.6 km, well inside the predicted interval. Constraints on the mass-radius relation for neutron stars and on the pressure-density relation of dense matter are also imposed in Ref. [18], where an empirical dense-matter equation of state is obtained from a set of seven neutron stars with well-determined distances (three type I x-ray bursters, three transient low-mass x-ray binaries, and one isolated cooling neutron star, RX J18563754). From the analysis of these seven objects, the authors predict a radius of 11–12 km for a star with a mass $1.4\ M_\odot$, which QMC does not satisfy, and conclude that the maximum mass is, in general, larger than $1.8\ M_\odot$. QMC predicts a the maximum star mass of $1.78\ M_\odot$, only slightly smaller than this value. Some of these constraints (i.e., the ones coming from the observation of compact stars) should still be considered with care either because the of the small number of studied objects or due to the uncertainty on the interpretation of the observations.

The QMC model was never applied before to describe warm stellar matter, present in protoneutron stars and, therefore, this is in this direction. We consider both neutrino-free matter and neutrino-trapped matter. The largest temperatures are attained after the neutrinos leave the star [21]. In Ref. [8], the effect of neutrino trapping on hybrid stars was studied, but only at zero temperature. Although one does not expect that the temperature of matter inside compact stars is uniform, these results are important in the calculations of stellar evolution. A more probable possibility for stellar matter is that the entropy is constant in the interior of compact stars and the temperature varies [21,22]. This calculation is also performed next. All results are compared with the ones obtained with the NLWM.

This article is organized as follows: In Sec. II, we give a brief review of the QMC model and its generalization for finite temperatures; in Sec. III, we present some results dealing with the description of warm nuclear matter within the QMC; in Sec. IV, we draw our final conclusions.

II. FORMALISM

In the QMC model, the nucleon in nuclear medium is assumed to be a static spherical MIT bag in which quarks interact with the scalar and vector fields σ, ω, and ρ; and these fields are treated as classical fields in the mean-field approximation [2,4]. The quark field $\psi_q(\mathbf{r}, t)$ inside the bag then satisfies the Dirac equation

$$\left[i\gamma \cdot \partial - (m_q 0 - V_\sigma) - \gamma 0\left(V_\omega + \tfrac{1}{2}\tau_{3q} V_\rho\right)\right]\psi_q(\mathbf{r}, t) = 0, \tag{1}$$

with $q = u,\ d,\ s$, where $V_\sigma = g_\sigma^q \sigma_0$, $V_\omega = g_\omega^q \omega_0$, and $V_\rho = g_\rho^q \rho_{03}$ with σ_0, ω_0, and ρ_{03} being the classical meson fields. The quantities g_σ^q, g_ω^q, and g_ρ^q are the quark-meson couplings with the σ, ω, and ρ mesons, respectively, and m_q^0 is the current quark mass. The normalized ground state for a quark in the bag is given by

$$\psi_q(\mathbf{r}, t) = \mathcal{N}_q \exp(-i\epsilon_q t/R_B) \begin{pmatrix} j_0\left(\frac{x_q r}{R_B}\right) \\ i\beta_q \vec{\sigma} \cdot \hat{r}\, j_1\left(\frac{x_q r}{R_B}\right) \end{pmatrix} \frac{\chi_q}{\sqrt{4\pi}}, \tag{2}$$

where $\hat{r} = \mathbf{r}/|r|$ and

$$\begin{aligned} \epsilon_q &= \Omega_q + R_B\left(V_\omega + m_\tau^q V_\rho\right), \\ \beta_q &= \sqrt{\frac{\Omega_q - R_B\, m_q^*}{\Omega_q + R_B\, m_q^*}}, \end{aligned} \tag{3}$$

with the normalization factor given by

$$\mathcal{N}_q^{-2} = 2R_B^3 j_0^2(x_q)[\Omega_q(\Omega_q - 1) + R_B m_q^*/2]/x_q^2, \tag{4}$$

where $\Omega_q \equiv \sqrt{x_q^2 + (R_B\, m_q^*)^2}$, $m_q^* = m_q^0 - g_\sigma^q\, \sigma_0$, R_B is the bag radius of baryon B, χ_q is the quark spinor, and $m_\tau^q = 1/2(-1/2)$ for quark u (d). The quantities ψ_q, ϵ_q, β_q, $\mathcal{N}_q$, Ω_q, and m_q^* all depend on the baryon considered.

The boundary condition at the bag surface is given by

$$i\gamma \cdot \hat{n}\psi_q = \psi_q, \tag{5}$$

where $\hat{n}$ is the unit vector normal to the surface. For this, the ground state reduces to

$$j_0(x_q) = \beta_q\, j_1(x_q), \tag{6}$$

which determines the dimensionless quark momentum x_q.

At finite temperatures, the three quarks inside the bag can be thermally excited to higher angular momentum states and, in addition, quark-antiquark pairs can be created. For simplicity, we assume that the bag describing the nucleon continues to remain in a spherical shape with radius R, which is now temperature dependent. The single-particle energies in units of R^{-1} are given as

$$\epsilon_q^{n\kappa} = \Omega_q^{n\kappa} + R_B\left(V_\omega + m_\tau^q V_\rho\right), \tag{7}$$

for the quarks and

$$\epsilon_{\bar{q}}^{n\kappa} = \Omega_q^{n\kappa} - R_B\left(V_\omega + m_\tau^q V_\rho\right), \tag{8}$$

for the antiquarks, where the + sign is for u quarks and − for d quarks, and

$$\Omega_q^{n\kappa} = \sqrt{x_{n\kappa}^2 + R_B^2 m_q^{*2}}. \tag{9}$$

In the above, the quark eigenvalues $x_{n\kappa}$ for the state characterized by n and κ are determined by the boundary condition at the bag surface. Thus, the quark eigenvalues $x_{n\kappa}$ become modified from the surrounding nucleon medium at finite temperature. The total energy from the quarks and antiquarks at finite temperature is

$$E_B^{\rm tot} = \sum_{q,n,\kappa} \frac{\Omega_q^{n\kappa}}{R_B} \left(f_{n\kappa}^q + f_{n\kappa}^{\bar q}\right), \tag{10}$$

where

$$\begin{aligned} f_{n\kappa}^q &= \frac{1}{e^{(\Omega_q^{n\kappa}/R_B - \nu_q)/T} + 1}, \\ f_{n\kappa}^{\bar q} &= \frac{1}{e^{(\Omega_q^{n\kappa}/R_B + \nu_q)/T} + 1}, \end{aligned} \tag{11}$$

with ν_q being the effective quark chemical potential, related to the quark chemical potential μ_q as

$$\nu_q = \mu_q - V_\omega - m_\tau^q V_\rho. \tag{12}$$

For a given temperature T, the effective quark chemical potentials ν_q are determined from the total number of quarks, isospin density, and strangeness:

$$n_0^j = \sum_{q,n,\kappa} \left(f_{n\kappa}^q - f_{n\kappa}^{\bar q}\right) \equiv 3, \tag{13}$$

$$n_3^j = \sum_{q,n,\kappa} 2m_\tau^q \left(f_{n\kappa}^q - f_{n\kappa}^{\bar q}\right) \equiv 2m_\tau^{(j)}, \tag{14}$$

$$r_s^j = \sum_{q,n,\kappa} r_s(q) \left(f_{n\kappa}^q - f_{n\kappa}^{\bar q}\right). \tag{15}$$

The energy of a static bag describing baryons consisting of three ground-state quarks can be expressed as

$$E_B^{\rm bag} = E_B^{\rm tot} - \frac{Z_B}{R_B} + \frac{4}{3}\pi R_B^3 B_B, \tag{16}$$

where Z_B is a parameter which accounts for zero-point motion and B_B is the bag constant. The entropy of the bag is defined as

$$\begin{aligned} \mathcal{S}_B^{\rm bag} = -\sum_{q,n,\kappa} \big[& f_{n\kappa}^q \ln f_{n\kappa}^q + \left(1 - f_{n\kappa}^q\right) \ln\left(1 - f_{n\kappa}^q\right) \\ & + \bar f_{n\kappa}^q \ln \bar f_{n\kappa}^q + \left(1 - \bar f_{n\kappa}^q\right) \ln\left(1 - \bar f_{n\kappa}^q\right) \big], \end{aligned} \tag{17}$$

and the free energy for the bag is given by

$$F_B^{\rm bag} = E_B^{\rm bag} - T S_B^{\rm bag}. \tag{18}$$

The set of parameters used in the present work is given in Ref. [7]. The effective mass of a nucleon bag at rest is taken to be

$$M_B^* = F_B^{\rm bag}, \tag{19}$$

differently from Ref. [4] where the bag energy was considered instead of the free energy to define the effective mass. The equilibrium condition for the bag is then obtained by minimizing the effective mass M_B^* with respect to the bag radius:

$$\frac{d\, M_B^*}{d\, R_B^*} = 0. \tag{20}$$

Once the bag radius is obtained, the effective baryon mass is immediately determined. The total energy density of baryonic matter at finite temperature T and at finite baryon density ρ is

$$\begin{aligned} \mathcal{E} = & \frac{2}{(2\pi)^3} \sum_B \int d^3k [\epsilon^* (f_B + \bar f_B) + \mathcal{V}_{0B} (f_B - \bar f_B)] \\ & + \frac{1}{2} m_\sigma^2 \sigma^2 - \frac{1}{2} m_\omega^2 \omega^2 - \frac{1}{2} m_\rho^2 \rho_{03}^2 \\ & + \sum_l \frac{\gamma_l}{(2\pi)^3} \int d^3k \left(k^2 + m_l^2\right)^{1/2} (f_l + \bar f_l), \end{aligned} \tag{21}$$

where $\gamma_l = 2\,(1)$ for electrons and muons (neutrinos), f_B and $\bar f_B$ are the thermal distribution functions for the baryons and antibaryons and f_l and $\bar f_l$ are the distribution functions for the leptons:

$$\begin{aligned} f_B &= \frac{1}{e^{(\epsilon^* - \nu_B)/T} + 1}, \quad \bar f_B = \frac{1}{e^{(\epsilon^* + \nu_B)/T} + 1}, \\ f_l &= \frac{1}{e^{(\epsilon_l - \mu_e)/T} + 1}, \quad \bar f_l = \frac{1}{e^{(\epsilon_l + \mu_e)/T} + 1}, \end{aligned} \tag{22}$$

where $\epsilon^* = (\vec k^2 + M_B^{*2})^{1/2}$ is the effective nucleon energy, $\nu_B = \mu_B - \mathcal{V}_{0B}$ is the effective baryon chemical potential, and $\mathcal{V}_{0B} = g_{\omega B}\omega + I_{3B}\, g_{\rho B} b_{03}$ (I_{3B} is the isospin projection of the baryon species B) and $\epsilon_l = (k^2 + m_l^2)^{1/2}$. The couplings of the mesons with the baryons $g_{\omega B}$ and $g_{\rho B}$ will be discussed below. The thermodynamic grand potential density and the free-energy density are defined as

$$\Omega = \mathcal{F} - \sum_B \mu_B \rho_B, \quad \mathcal{F} = \mathcal{E} - T\mathcal{S}, \tag{23}$$

with the entropy density $\mathcal{S} = S/V$ is given by

$$\begin{aligned} \mathcal{S} = -\sum_B \frac{2}{(2\pi)^3} \int d^3k [& f_B \ln f_B + (1 - f_B) \ln(1 - f_B) \\ & + \bar f_B \ln \bar f_B + (1 - \bar f_B) \ln(1 - \bar f_B)]. \end{aligned} \tag{24}$$

The baryon density (of each baryon species) is given by

$$\rho_B = \frac{2}{(2\pi)^3} \int d^3k (f_B - \bar f_B), \tag{25}$$

so that the total baryon density is $\rho = \sum_B \rho_B$. The pressure is the negative of Ω which, after an integration by parts, can be written as

$$\begin{aligned} P = & \frac{1}{3} \sum_B \frac{2}{(2\pi)^3} \int d^3k \frac{\mathbf{k}^2}{\epsilon^*} (f_B + \bar f_B) \\ & - \frac{1}{2} m_\sigma^2 \sigma^2 + \frac{1}{2} m_\omega^2 \omega^2 + \frac{1}{2} m_\rho^2 \rho_{03}^2 \\ & + \frac{1}{3} \sum_l \frac{\gamma_l}{(2\pi)^3} \int d^3k \frac{\mathbf{k}^2}{\left(k^2 + m_l^2\right)^{1/2}} (f_l + \bar f_l). \end{aligned} \tag{26}$$

From the above expression, the pressure depends explicitly on the meson mean fields σ, ω, and ρ_{03}. It also depends on

the baryon effective mass M_B^* which, in turn, also depends on the sigma field [see Eqs. (10)–(20)]. At a given temperature and for a given baryon density, the effective mass is known for given values of the meson fields, once the bag radius R_B and the effective quark chemical potentials ν_q are calculated by using Eqs. (13)–(15). The meson fields σ, ω_0, and ρ_{03} are determined through

$$\frac{\partial P}{\partial \sigma} = \left(\frac{\partial P}{\partial M_N^*}\right)_{\mu_i,T} \frac{\partial M_N^*}{\partial \sigma} + \left(\frac{\partial P}{\partial \sigma}\right)_{M_N^*} = 0, \quad (27)$$

$$m_\omega^2 \omega_0 = \sum_B g_{\omega B} \rho_B, \quad (28)$$

$$m_\rho^2 \rho_{03} = \sum_B g_{\rho B} I_{3B} \rho_B. \quad (29)$$

The hyperon couplings are not relevant to the ground-state properties of nuclear matter, but information about them can be available from the levels in hypernuclei [23–28]:

$$g_{\sigma B} = x_{\sigma B} g_{\sigma N}, \quad g_{\omega B} = x_{\omega B} g_{\omega N}, \quad g_{\rho B} = x_{\rho B} g_{\rho N},$$

and $x_{\sigma B}$, $x_{\omega B}$, and $x_{\rho B}$ are equal to 1 for the nucleons and acquire different values in different parametrizations for the other baryons. Note that the s-quark is unaffected by the sigma and omega mesons (i.e., $g_\sigma^s = g_\omega^s = 0$).

We have fixed the $x_{\omega B}$ value from the hyperon potentials in nuclear matter, $U_B = -(M_B^* - M_B) + x_{\omega B} g_{\omega N} \omega_0$, for $B = \Lambda$, Σ, and Ξ to be -28, 30, and -18 MeV, respectively. We found that $x_{\omega\Lambda} = 0.743$, $x_{\omega\Sigma} = 1.04$, and $x_{\omega\Xi} = 0.346$. We fixed the $x_{\rho B} = 1$ for all the baryons.

The composition of the stelar matter is determined by the requirements of the charge neutrality and chemical equilibrium under the weak processes for trapped neutrinos:

$$\mu_B = \mu_n - q_B(\mu_e - \mu_{\nu_e}), \quad (30)$$

where q_B is the baryon electric charge. For charge neutrality, we must have

$$\sum_B q_B \rho_B + \sum_l q_l \rho_l = 0, \quad (31)$$

where q_l is the lepton charge. In neutrino-free matter, μ_{ν_e} is set to zero in the above equation.

For the bag radius, we take $R_N = 0.6$ fm. The two unknowns Z_N and B_N are obtained by fitting the nucleon mass $M = 939$ MeV and enforcing the stability condition for the bag at free space. The values obtained are $Z_N = 4.005\,06$ and $B_N^{1/4} = 210.854$ MeV for $m_u = m_d = 5.5$ MeV. Next, we fit the quark-meson coupling constants g_σ^q, $g_\omega = 3g_\omega^q$, and $g_\rho = g_\rho^q$ for the nucleon to obtain the correct saturation properties of the nuclear matter, $E_N \equiv \mathcal{E}/\rho - M = -15.7$ MeV at $\rho = \rho_0 = 0.15$ fm^{-3}, $a_{\rm sym} = 32.5$ MeV, $K = 257$ MeV and $M^* = 0.774M$. We next present our results.

III. RESULTS

In this section, we discuss the effect of temperature on the EOS of warm stellar matter both neutrino free and with trapped neutrinos. We consider a fixed temperature and also a fixed entropy as suggested by supernova simulations [22]. The effect of temperature on the particle yields is also discussed. Finally, we present the mass and radius properties of stars described by the EOS we have obtained.

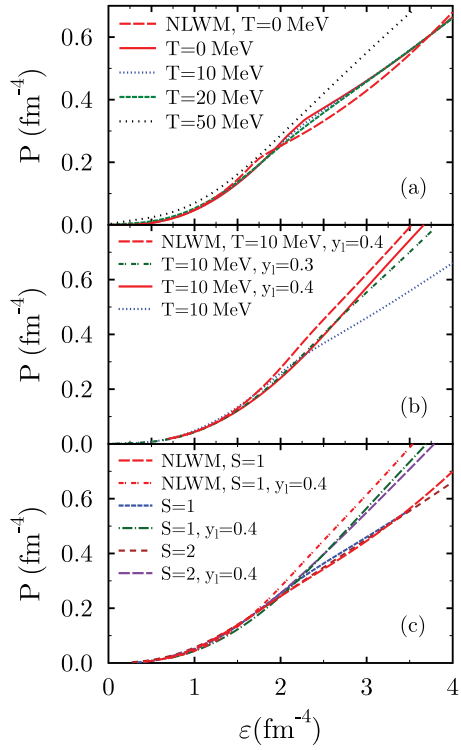

FIG. 1. (Color online) EOS for (a) different temperatures, (b) $T = 10$ MeV and different lepton fractions, and (c) fixed entropy per baryon ($S = 1$ and 2) and different lepton fractions. QMC was used for all temperatures and entropies. For comparison, some results obtained with the GM1 parametrization of NLWM are also included.

In Fig. 1, the EOS is shown for different cases. In Fig. 1(a) four temperatures are considered for neutrino-free matter in β equilibrium. One can see that the EOS does not vary considerably up to $T = 20$ MeV, but it becomes much harder at $T = 50$ MeV. The softening that occurs in the range $2 < \mathcal{E} < 3$ fm^{-4} is due to the onset of hyperons at lower densities for finite temperatures. In Fig. 1(b) three EOS are shown for $T = 10$ MeV: one for neutrino-free matter and the others for matter with neutrinos and different lepton fractions. The neutrinos make the EOS harder above $\mathcal{E} = 2.5$ fm^{-4} after the onset of hyperons. This happens because the onset of hyperons occurs with a reduction of the electron fraction and, therefore, a strong increase in neutrinos. However, below that energy density, when only nucleonic degrees of freedom are present, the EOS is softer. This occurs because the presence of neutrinos lowers the fraction of neutrons [21] and, therefore, the neutron pressure. In Fig. 1(c), the EOS for neutrino-free matter and matter with a lepton fraction equal to 0.4 are displayed for fixed entropies per baryon $S = 1$ and $S = 2$. There is not a large difference between $S = 1$ and $S = 2$ EOS: at low densities the $S = 1$ EOS is softer but, for the larger densities, the opposite occurs because of an earlier onset of the hyperons for the larger entropy. The amount of leptons is more important than the entropy in establishing the softness

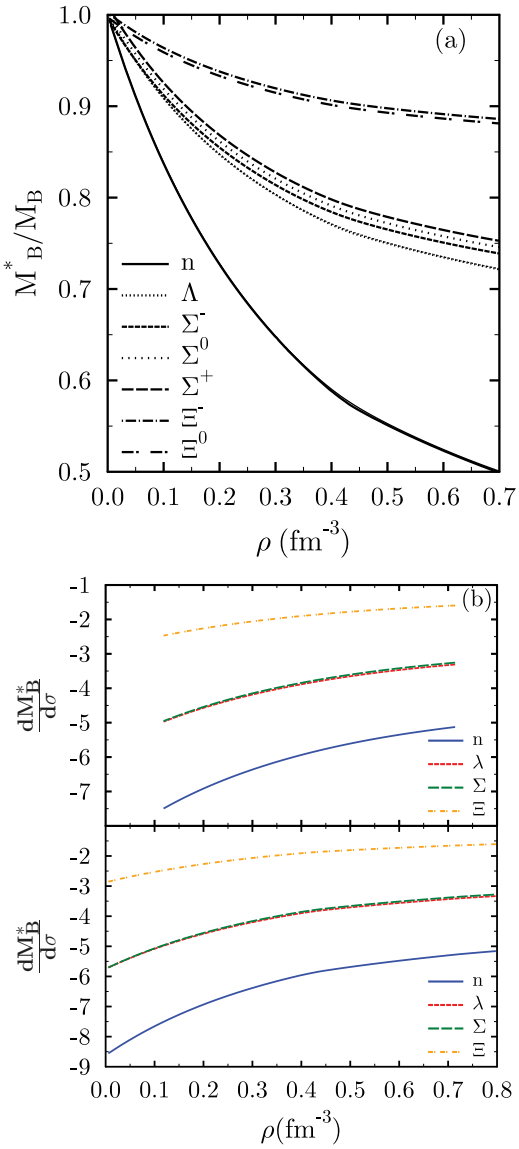

FIG. 2. (Color online) Baryons' effective mass: (a) effective mass of the baryons at $T = 10$ MeV; (b) derivative of the effective mass with respect to sigma versus baryon density at $T = 10$ MeV (top) and at $T = 0$ MeV (bottom).

or hardness of the EOS. The presence of neutrinos shifts the onset of hyperons to larger densities.

In Fig. 2(a), the baryon effective masses are shown for $T = 10$ MeV. Contrary to what was found in Ref. [4], they never reach values above their free masses. The differences are due to the choice of the bag free energy (instead of the bag energy) in defining the effective masses. The curves for the effective masses at zero temperature are practically indistinguishable from the ones at 10 MeV (differences are of the order of 1 MeV) and hence they are not shown. A figure with the effective masses at different temperatures is shown in Ref. [5], from where we can see that the masses do not vary much up to 50 MeV but, for higher temperatures, the decrease in the mass is quite large. In Ref. [29], the same prescription given in Ref. [4] was used and, even so, the effective masses came out below the free masses. This is a result we do not understand and did not obtain when the quark-medium-dependent energy levels are determined self-consistently. In the present work, we have made a completely self-consistent calculation using all the internal levels necessary to get convergence in the sums that involve the quark degrees of freedom.

In Fig. 2(b), we show the derivative of the effective mass with respect to the sigma field at $T = 0$ and $T = 10$ MeV. For low densities, the derivative seems to be proportional to the number of u and d quarks: 7.5 (n), 5 (Λ, Σ), and 2.5 (Ξ). For larger densities, there is a deviation from this trend. These derivatives indicate that the effective masses are not linear in the sigma field or, equivalently, that the sigma coupling constant decreases with density. We have verified that the ratio between the hyperon masses and the nucleon masses is almost constant: 0.66 for Λ and Σ and 0.32 for Ξ. Only a slight decrease of the order of 4% (8%) is observed for Λ/Σ (Ξ) in the range $0 < \rho < 0.8$ fm^{-3}. A smaller decrease rate of the hyperons at large densities does not favor their formation as much as in the NLWM at high densities, as can be confirmed from Fig. 8, where it is seen that the slope of the NLWM curves (strangeness fraction versus density) are larger than the corresponding QMC curves.

In Fig. 3, we display the effective baryon radii at $T = 10$ MeV. It is seen that they decrease with density. The larger differences occur for the lighter baryons. The same behavior was obtained at zero temperature. In Ref. [30], a swelling of the nucleons in the nuclear medium was predicted. This swelling is due to the medium modification of the meson cloud of the nucleon. However, as referred to in Ref. [31], the swelling is due to the presence of a bath of pions which surrounds the nucleon. Models that do not consider dressed nucleons, like QMC, do not predict nucleon swelling. In Ref. [5], it was shown that the radii increase with increasing temperature. However, for $T = 20$ MeV or below, the differences are negligible.

In Figs. 4, 5, 6, and 7, we show the particle fractions in four different situations. In Fig. 4, baryon fractions are shown for neutrino-free matter at $T = 0$ and 10 MeV. Due to the hyperon-meson coupling constants chosen, the onset of the

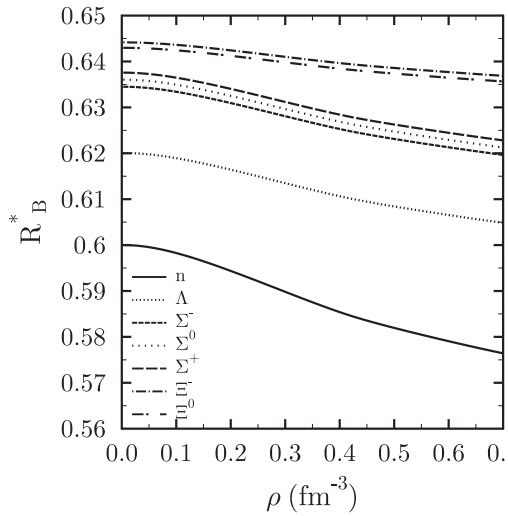

FIG. 3. Effective radius of the baryons at $T = 10$ MeV.

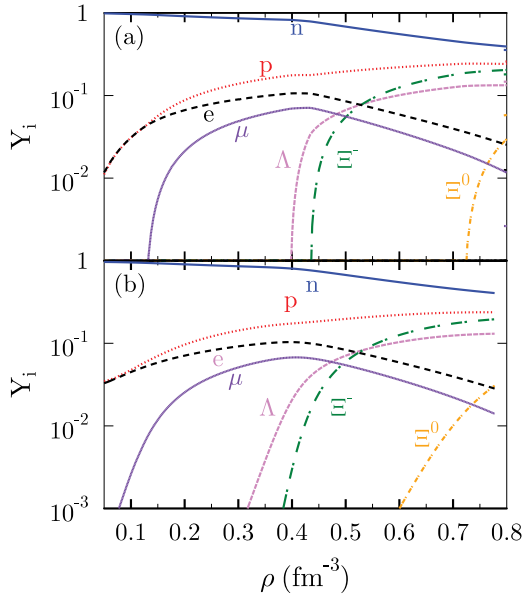

FIG. 4. (Color online) QMC particle yields at finite temperature: (a) at $T = 0$ MeV and (b) at $T = 10$ MeV.

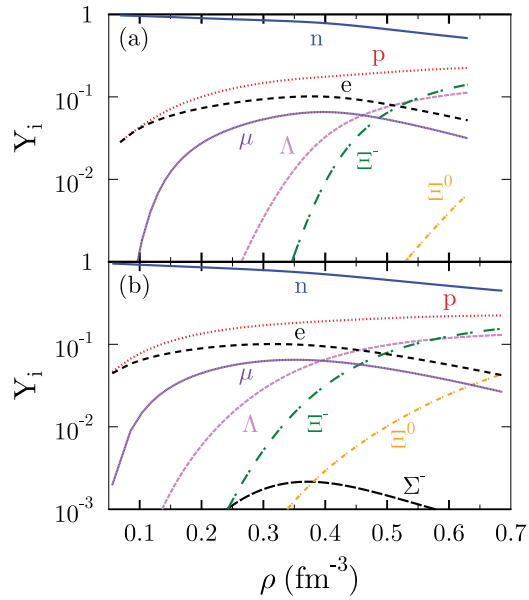

FIG. 6. (Color online) QMC particle yields for fixed entropy of (a) $S = 1$ and (b) $S = 2$.

Σ is shifted to larger densities and so is not shown on the plot. Λ is the first hyperon to appear, immediately followed by Ξ^-. The negative charge of this hyperon compensates for its large mass. The onset of the heavier baryons occurs at lower densities as the temperature increases. Below, we discuss how the strangeness fraction depends on the temperature.

In Fig. 5, the baryon fractions are shown for matter with trapped neutrinos at a fixed temperature and two different lepton fractions: 0.3 and 0.4. The larger the lepton fraction, the later the onset of hyperons takes place. Different fixed lepton fractions influence the particle yields through the chemical potentials. The appearance of negatively charged hyperons reduces the electron fraction and, therefore, increases the neutrino fraction.

In Fig. 6, the baryon fractions are shown for neutrino-free matter at fixed entropy per baryon ($S = 1$ and 2). The effect of increasing the entropy is similar to the effect of increasing the temperature, as can be checked in Fig. 4 (i.e., hyperons appear at lower densities for higher entropies). For $S = 2$, even the Σ^- is present, although in very small amounts.

Finally, in Fig. 7 we display the particle yields in matter with trapped neutrinos at fixed entropy per particle. We have considered a lepton fraction of 40% and the entropies per particle $S = 1$ and $S = 2$. As already discussed for a fixed

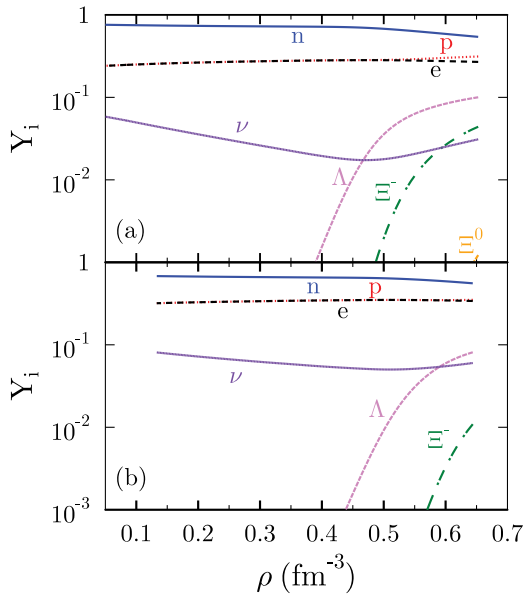

FIG. 5. (Color online) QMC particle yields at $T = 10$ MeV for fixed lepton fraction (a) $y_l = 0.3$ and (b) $y_l = 0.4$.

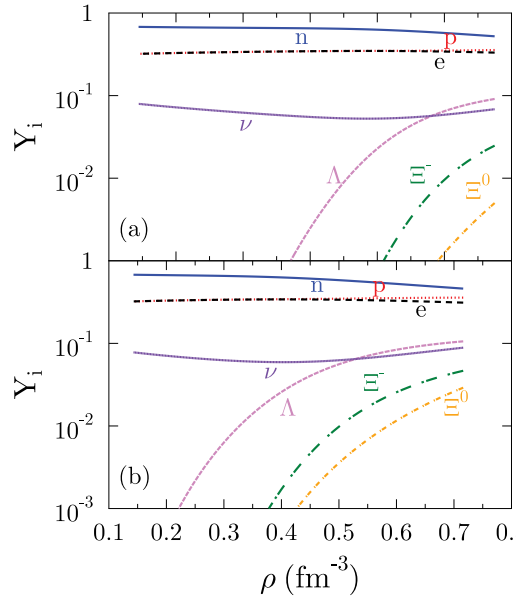

FIG. 7. (Color online) QMC particle yields for fixed entropy and lepton fractions of (a) $S = 1$ and $y_l = 0.4$ and (b) $S = 2$ and $y_l = 0.4$.

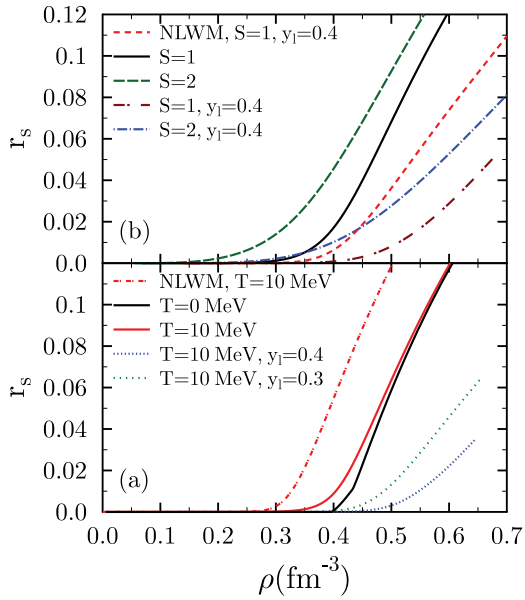

FIG. 8. (Color online) QMC strangeness fraction versus density for different entropies and temperatures. For comparison, some GM1 results are also included.

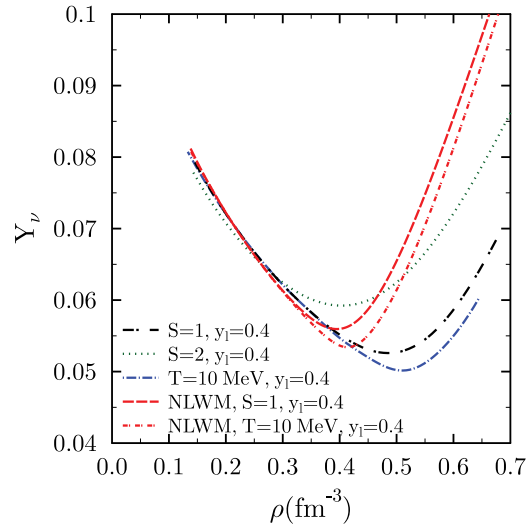

FIG. 9. (Color online) Neutrino yields for fixed lepton fraction.

temperature, the presence of neutrinos shifts the hyperon onset to larger densities. It is also seen that a larger entropy favors the onset of hyperons at smaller densities and a larger hyperon fraction.

The effect of temperature on the strangeness fraction is best discussed analyzing Fig. 8. In this figure, we have plotted, for fixed entropy and fixed temperature, the fraction of strangeness in the system

$$r_s = \frac{\sum_B q_{sB}\rho_B}{3\rho}, \tag{32}$$

where q_{sB} is the strangeness charge. At fixed entropy, one can see that a system with $S = 2$ carries more strangeness than a system with $S = 1$, and the strange particles appear at lower densities. This reflects the particle yields already discussed in Figs. 6 and 7. Although the onset of strangeness occurs at lower densities for the larger entropy per baryon, for the larger densities the differences between different entropy values decrease. For comparison we have also included the strangeness fraction obtained for $S = 1$ with the GM1 parametrization [25] of the NLWM and the hyperon-meson couplings fitted to the same hyperon potentials in nuclear matter [28]. It is seen that, within QMC, less strange particles are produced and they appear at higher densities. This is due to the fact that the EOS with only nucleon degrees of freedom is softer for QMC than GM1.

If fixed temperatures are considered [see Fig. 8(a)], one concludes that strangeness is enhanced with the increase of temperature and its onset occurs at smaller densities. However, comparing $T = 0$ with $T = 10$ MeV neutrino-free matter, it is seen that, for $\rho \sim 0.5$ fm^{-3} and above, the strangeness fractions almost coincide. For $T = 10$ MeV, GM1 predicts a much larger strangeness fraction. We also observe that neutrino-free systems carry more strangeness than systems with fixed lepton fractions, and the higher the lepton fraction, the less strange particles are present. Figure 8 summarizes the conclusions taken from Figs. 4–7 with the particle yields.

The strangeness fraction for matter with trapped neutrinos is closely related with the neutrino fraction: larger strangeness fractions imply smaller electron fractions and, therefore, larger neutrino fractions when the total lepton fraction is fixed. This is seen in Fig. 9, where the neutrino fractions for a fixed $y_l = 0.4$ and different situations; namely, $S = 1$ and 2 with QMC, and $T = 10$ MeV and $S = 1$ within QMC and GM1, are shown. The neutrino fraction is larger for a higher fixed entropy since there are also more hyperons for the larger entropy. For a fixed entropy of $S = 1$, the neutrino fraction reaches a minimum at higher densities for QMC as compared with the NLWM and retains smaller values for densities above the minimum. This is again due to the fact that, for QMC, the strangeness onset occurs at larger densities and remains smaller. The behavior below the minimum reflects the properties of the nucleonic EOS: a larger proton fraction corresponds to a larger electron fraction and a smaller neutrino fraction. Similar conclusions are obtained when comparing QMC and GM1 at the same temperature ($T = 10$ MeV).

In Fig. 10, the temperature of the system is shown for fixed entropies $S = 1$ and $S = 2$ both for neutrino-free and neutrino-trapped matter. A system with higher entropy reaches higher temperatures, but never higher than 35 MeV for the densities shown and $S \leqslant 2$. The full green curves are obtained for neutrino-free matter. They show a softening when the hyperons set on: for fixed entropy, temperature cannot rise so fast when the number of degrees of freedom increases. The softening of the temperature curve is larger for GM1 and occurs at smaller densities because the strangeness fraction is larger and its onset occurs at smaller densities. This softening does not occur, or is much smaller, for matter with trapped neutrinos due to the late onset of hyperons. A comparison of GM1 and QMC at small densities shows that temperature rises more steeply for GM1 both for neutrino-free and neutrino-trapped matter. This mainly reflects the differences between the nucleonic QMC and GM1 EOS; namely, the larger effective masses predicted

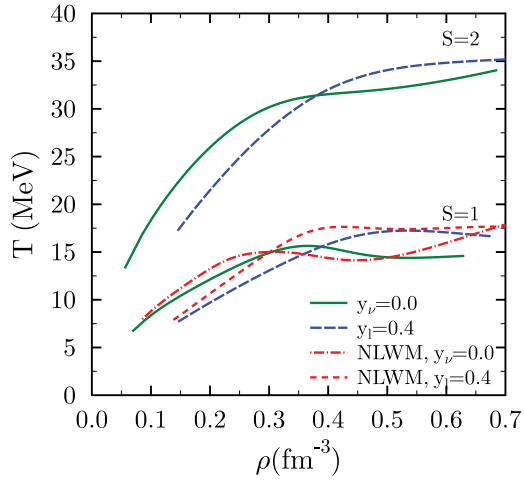

FIG. 10. (Color online) Temperature versus density. For comparison, some GM1 results are also included.

by QMC. The temperature of a multicomponent Fermi gas system at fixed entropy is given by [32]

$$T = \frac{S}{\pi^2} \sum_i \frac{p_{Fi}^3}{p_{Fi}\sqrt{p_{Fi}^2 + M_{Fi}^{*\,2}}}.$$

Larger effective masses correspond to smaller temperatures. From this expression it is also seen that increasing the degrees of freedom makes the temperature increase more slowly because the Fermi momenta of the system components decrease. The temperature oscillates differently in the QMC model from the NLWM, but the overall numbers are similar.

Neutrino chemical potentials are shown for different situations in Fig. 11. The values of the neutrino chemical potentials reflect their abundances: for a fixed temperature the NLWM produces neutrinos with much higher chemical potentials for densities above hyperon onset. For $S = 2$, below hyperon onset, neutrino fractions are smaller due to larger proton and, therefore, electron fractions. This is reflected in the smaller

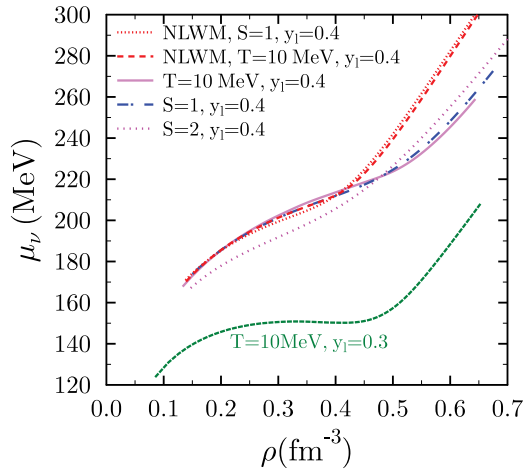

FIG. 11. (Color online) Neutrino chemical potential versus density. For comparison, some GM1 results are also included.

TABLE I. Stellar properties at different temperatures and entropies per baryon. QMC and the GM1 parametrization of the NLWM have been used.

Model	$M_{\rm max}(M_\odot)$	$M_b(M_\odot)$	R(km)	ε_0(fm^{-4})
QMC ($T = 0$)	1.78	2.02	12.65	4.63
QMC ($T = 10$ MeV)	1.78	2.01	12.89	4.49
QMC ($T = 20$ MeV)	1.79	2.00	14.48	4.52
QMC ($S = 1$)	1.78	1.98	12.81	4.61
QMC ($S = 2$)	1.78	1.95	13.22	4.60
QMC ($S = 1$, $y_l = 0.4$)	1.92	2.04	11.68	4.38
QMC ($S = 2$, $y_l = 0.4$)	1.94	2.01	11.85	4.78
NLWM ($T = 0$ MeV)	1.77	2.00	12.02	5.65
NLWM ($T = 10$ MeV)	1.78	2.00	12.20	5.63
NLWM ($T = 20$ MeV)	1.79	2.01	13.42	5.31
NLWM ($S = 1$)	1.78	2.00	12.13	5.52
NLWM ($S = 2$)	1.80	1.98	12.37	5.27
NLWM ($S = 1$, $y_l = 0.4$)	2.06	2.28	12.13	5.37
NLWM ($S = 2$, $y_l = 0.4$)	2.06	2.23	12.31	5.18

neutrino chemical potentials obtained (dotted line). We also compare neutrino chemical potentials for different lepton fractions, namely 0.3 and 0.4. A smaller lepton fraction implies a smaller neutrino fraction and, therefore, smaller neutrino chemical potentials.

The radii, gravitational, and baryonic masses of compact stars are calculated by the integration of the Tolman-Oppenheimer-Volkoff (TOV) equations, which use as input the EOS obtained with the QMC model. The results are shown in Table I and Figs. 12–14. We also include the corresponding results obtained with the GM1 parametrization of the NLWM for comparison.

Temperature does not strongly effect the maximum gravitational mass and the baryonic maximum mass decreases slightly with temperature or entropy. Similar conclusions were obtained in Ref. [21]. For a neutrino-free star, the radius of the maximum mass increases with temperature. This occurs because the EOS becomes harder when temperature increases. Central energy densities of maximum-mass configurations are $\sim$1 fm^{-4} smaller in QMC than GM1: the larger hyperon

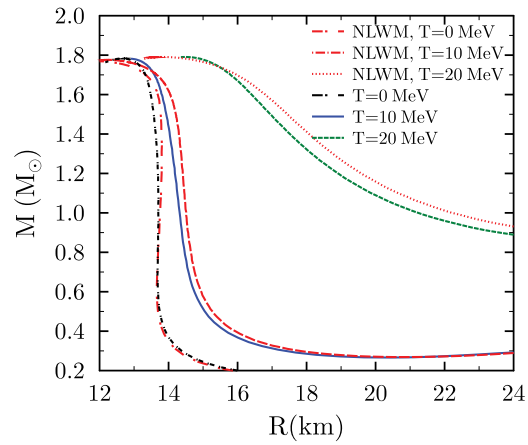

FIG. 12. (Color online) Neutron star radius versus mass at $T = 0$, 10, and 20 MeV for QMC and GM1.

fraction in the core of the star for GM1 is the reason for this behavior. This is also the cause of the larger radius in QMC.

One important difference between QMC and GM1 is the window of metastability. If we consider that the star evolves from a configuration with $S = 1$ and trapped neutrinos to a warmer neutrino-free configuration with $S = 2$ before it cools, we see that a set of stars close to the maximum-mass configuration with trapped neutrinos will decay to a low-mass blackhole during cooling. For GM1, this is a window with 0.3 $M_\odot$ baryonic mass, whereas for QMC it is smaller, $\sim$0.1 $M_\odot$. This is a consequence of the much smaller hyperon fraction and, therefore, neutrino fraction in QMC stars with trapped neutrinos. In fact, a star with no hyperons has a smaller maximum mass in a configuration with trapped neutrinos than in a neutrino-free configuration [21].

Next, we first discuss the effect of temperature on the mass-radius graph of compact stars for fixed temperature, although supernova simulations seem to show that it is a good approximation to consider that stars have a uniform entropy per baryon and not a uniform temperature [22]. QMC stars show a similar behavior to GM1 stars, although there are some differences. QMC model predicts smaller radii for stars with masses below 1.7 $M_\odot$, because QMC has a softer EOS. However, this is no longer the case for the most massive stars because these have a core with a smaller fraction of hyperons within QMC.

The trend is the same for a fixed entropy per baryon, as seen in Fig. 13, where the mass-radius graph of the families of stars obtained with QMC and GM1 for an entropy per baryon $S = 1$ and 2 is shown. Except for the most massive stars, the radii of the QMC stars are smaller. It is only above 1.5 $M_\odot$ masses that GM1 stars have a core which contains hyperons, while for QMC stars this occurs for mass larger than 1.6 $M_\odot$. The larger fraction of hyperons in the core of GM1 maximum-mass configurations gives rise to larger central-energy densities and smaller radii.

Figure 14 allows a clearer discussion on the metastability of QMC stars with hyperons. In order for metastability to occur, a stable star that cools down should end up in a configuration with the same baryonic mass which is not stable. Comparing

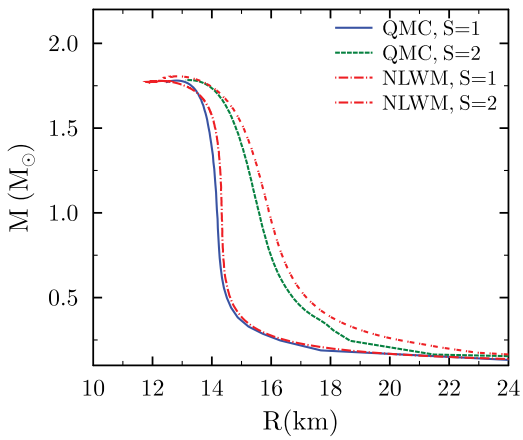

FIG. 13. (Color online) Neutron star radius versus mass for $S = 1$ for QMC and GM1.

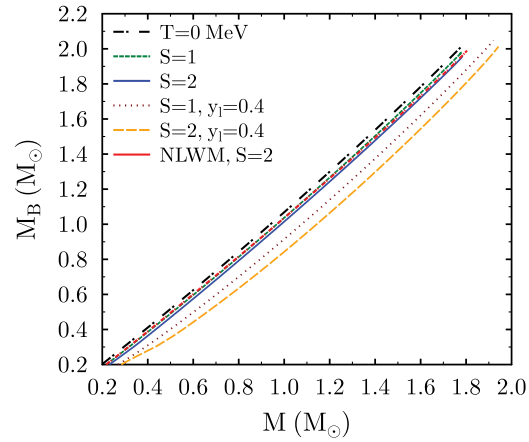

FIG. 14. (Color online) Baryonic mass versus gravitational mass of neutron star for QMC model.

the neutrino-free configurations for $S = 0$, 1, and 2, it is seen that the maximum baryonic mass configuration occurs at $S = 0$ and, therefore, no metastability occurs during the cooling down of a neutrino-free star. However, the same is not true for stars with trapped neutrinos: there is a set of configurations for $S = 1$ with trapped neutrinos that have a larger baryonic mass than the maximum stable baryonic mass of a neutrino-free star with $S = 2$. These are the metastable stars that will decay into a low-mass blackhole during cooling.

In Ref. [33], the threshold densities for the appearance of the hyperons in neutrons stars ($T = 0$) were obtained. The underlying calculation was based on effective single-particle potentials in the Hartree-Fock approximation and a set of available hyperon-nucleon interactions. It was shown that, although the results are model dependent, strangeness always appears around twice the saturation density. In their calculation, Σ^- was always the first hyperon to appear. However, from an experimental point of view, the Λ-nucleon interaction is better constrained. For this hyperon, they have obtained a larger onset density $2 \lesssim \rho \lesssim 3.5$ fm^{-3}. In our case, the first hyperon (Λ) appears at $2.66\rho_0$ and the second one to appear is the Ξ because we have considered a repulsive potential for the Σ^-. Moreover, the authors of Ref. [33] claim that strangeness cannot be ignored in the interior of neutron stars and confirm the already well-known consequences on their mass and radius. However, contrary to the calculation presented in Ref. [33], we predict much larger maximum star masses. These could be a consequence of the fact that three-body hyperon forces were not included.

IV. CONCLUSIONS

In the present work, we have investigated warm stellar matter present in protoneutron stars in the framework of the QMC model at finite temperatures. The EOS for warm hadronic matter with hyperon degrees of freedom was calculated at fixed temperatures and fixed entropy per particle (variable temperature) and the respective matter properties, particle fractions, and strangeness content were obtained and discussed both for neutrino-free matter and matter with trapped neutrinos.

A prescription for the calculation of the baryons effective masses in terms of the free energy was used, which enabled us to apply the QMC model for finite temperature once the baryon effective masses turned out to behave as expected.

The hyperon potentials in nuclear matter have been used to fix the coupling constants of the hyperons to the ω meson. The σ meson couplings are determined self-consistently from the effective-hyperon-mass calculation. For the hyperon potentials in nuclear matter we took $U = -28$, 30, and -18 MeV, respectively, for Λ, Σ, and Ξ. We considered the same coupling constant to the ρ meson for all baryons.

All results were compared with the ones obtained with the GM1 parametrization of the nonlinear Walecka model. The differences between both models are mainly due to the softer QMC EOS and the larger effective masses it predicts. As a consequence, the hyperon onset occurs at larger densities for QMC and a smaller neutrino fraction is obtained for matter with trapped neutrinos at a fixed lepton fraction. These differences certainly influence the development of the neutron star during cooling. In particular, it was shown that the window of metastability for the conversion into a low-mass blackhole during cooling is much smaller than the one obtained with the NLWM.

Similar conclusions had already been found at zero temperature in Ref. [14], where it was shown that the softness of the QMC model gave rise to high critical masses and a small window for metastability to conversion to a quark star.

ACKNOWLEDGMENTS

This work was partially supported by FCT and FEDER (Portugal) under the project FCOMP-01-0124-FEDER-008393 with FCT reference CERN/FP/109316/2009, by CNPq (Brazil), Capes/FCT n. 232/09 bilateral collaboration, and by Compstar, an ESF Research Networking Programme.

[1] B. Serot and J. D. Walecka, Adv. Nucl. Phys. **16**, 1 (1986).
[2] P. A. M. Guichon, Phys. Lett. B **200**, 235 (1988); K. Saito and A. W. Thomas, *ibid.* **327**, 9 (1994); K. Tsushima, K. Saito, A. W. Thomas, and S. V. Wright, *ibid.* **429**, 239 (1998).
[3] A. Chodos, R. L. Jaffe, K. Johnson, C. B. Thorne, and V. F. Weisskopf, Phys. Rev. D **9**, 3471 (1974).
[4] P. K. Panda, A. Mishra, J. M. Eisenberg, and W. Greiner, Phys. Rev. C **56**, 3134 (1997); P. K. Panda, R. Sahu, and C. Das, *ibid.* **60**, 038801 (1999); P. K. Panda, G. Krein, D. P. Menezes, and C. Providência, *ibid.* **68**, 015201 (2003).
[5] P. K. Panda, D. P. Menezes, and C. Providência, Phys. Rev. C **80**, 014905 (2009).
[6] S. Pal, M. Hanauske, I. Zakout, H. Stocker, and W. Greiner, Phys. Rev. C **60**, 015802 (1999).
[7] P. K. Panda, D. P. Menezes, and C. Providência, Phys. Rev. C **69**, 025207 (2004).
[8] D. P. Menezes and C. Providência, Phys. Rev. C **69**, 045801 (2004).
[9] D. P. Menezes, P. K. Panda, and C. Providência, Phys. Rev. C **72**, 035802 (2005).
[10] P. Yue and H. Shen, Phys. Rev. C **74**, 045807 (2006).
[11] P. Yue and H. Shen, Phys. Rev. C **77**, 045804 (2008).
[12] Ignazio Bombaci, Prafulla K. Panda, Constança Providência, and Isaac Vidaña, Phys. Rev. D **77**, 083002 (2008).
[13] Alexandre M. Santos, Constança Providência, and Prafulla K. Panda, Phys. Rev. C **79**, 045805 (2009).
[14] Isaac Vidaña, Constança Providência, Artur Polls, and Arnau Rios, Phys. Rev. C **80**, 045806 (2009).
[15] Bao-An Li, Lie-Wen Chen, and Che Ming Ko, Phys. Rep. **464**, 113 (2008).
[16] T. Klähn *et al.*, Phys. Rev. C **74**, 035802 (2006).
[17] K. Hebeler, J. M. Lattimer, C. J. Pethick, and A. Schwenk, arXiv:1007.1746 [nucl-th].
[18] A. W. Steiner, J. M. Lattimer, and E. F. Brown, arXiv:1005.0811 [astro-ph.HE].
[19] P. Danielewicz, R. Lacey, and W. G. Lynch, Science **298**, 1592 (2002).
[20] C. J. Horowitz and J. Piekarewicz, Phys. Rev. Lett. **86**, 5647 (2001); B. G. Todd-Rutel and J. Piekarewicz, *ibid.* **95**, 122501 (2005).
[21] M. Prakash, I. Bombaci, Manju Prakash, P. J. Ellis, J. M. Lattimer, and R. Knorren, Phys. Rep. **280**, 1 (1997).
[22] A. Burrows and J. M. Lattimer, Astrophys. J. **307**, 178 (1986).
[23] R. E. Chrien and C. B. Dover, Annu. Rev. Nucl. Part. Sci. **39**, 113 (1989).
[24] S. A. Moszkowski, Phys. Rev. D **9**, 1613 (1974); N. K. Glendenning and S. A. Moszkowski, Phys. Rev. Lett. **67**, 2414 (1991).
[25] N. K. Glendenning, *Compact Stars* (Springer-Verlag, New York, 2000).
[26] J. Schaffner-Bielich and A. Gal, Phys. Rev. C **62**, 034311 (2000).
[27] J. Schaffner-Bielich, M. Hanauske, H. Stöcker, and W. Greiner, Phys. Rev. Lett. **89**, 171101 (2002).
[28] M. Chiapparini, M. E. Bracco, A. Delfino, M. Malheiro, D. P. Menezes, and C. Providência, Nucl. Phys. A **826**, 178 (2009).
[29] I. Zakout and H. R. Jaqaman, Phys. Rev. C **59**, 962 (1999).
[30] G. E. Brown, C. B. Dover, P. B. Siegel, and W. Weise, Phys. Rev. Lett. **60**, 2723 (1988).
[31] G. Kalbermann, J. M. Eisenberg, and B. Svetitsky, Nucl. Phys. A **600**, 436 (1996); J. Dey and J. M. Eisenberg, Phys. Lett. B **334**, 290 (1994).
[32] A. W. Steiner, M. Prakash, and J. M. Lattimer, Phys. Lett. B **486**, 239 (2000).
[33] H. Dapo, B. J. Schaefer, and J. Wambach, Phys. Rev. C **81**, 035803 (2010).